Journal of Magnetic Resonance **144,** 357–366 (2000)
doi:10.1006/jmre.2000.2066, available online at http://www.idealibrary.com on IDEAL®

The Multidimensional Filter Diagonalization Method

II. Application to 2D Projections of 2D, 3D, and 4D NMR Experiments

Haitao Hu, Anna A. De Angelis, Vladimir A. Mandelshtam, and A. J. Shaka[1]

Chemistry Department, University of California, Irvine, California 92697-2025

Received August 4, 1999; revised March 1, 2000

The theory of the multidimensional filter diagonalization method (FDM) described in the previous paper (V. A. Mandelshtam, 2000, *J. Magn. Reson.* **144, 343–356 (2000)) is applied to NMR time signals with up to four independent time variables. Direct projections of the multidimensional time signals produce new kinds of 2D spectra. The resolution obtained by FDM can be far superior to that obtained by conventional phase-sensitive FT processing, and correlation peaks in heteronuclear and homonuclear experiments can be condensed to sharp singlets, removing all spin–spin couplings. Examples of** *singlet***-HSQC and** *singlet***-TOCSY spectra show big gains in resolution. It is not necessary to have a finely digitized spectrum, in which the individual multiplet components are resolved, for the methods to work. Examples of FDM spectra, ranging from simple organic molecules and steroids to metalloproteins, are shown.**

INTRODUCTION

The two fundamental problems of resolution and sensitivity continue to attract the attention of NMR spectroscopists confronting difficult, crowded spectra of small amounts of material. Gains in sensitivity accompany each new advance in NMR probe technology, radiofrequency (RF) preamplifier design, and attainable magnetic field strength. By contrast, fundamental resolution is now limited solely by advances in high-field magnet technology. Engineering advances in probe design have delivered a factor of 2 improvement in sensitivity during the last decade of this century, with cooled probe assemblies offering the promise of an additional gain of about 4. However, the highest attainable stable, homogeneous magnetic fields are only about 25% greater over the same time frame, and the cost of such magnets is expected to remain extremely high.

Two-dimensional (2D) Fourier transform (FT) NMR, as is well known, can offer a tremendous improvement in *effective* resolution by dispersing overlapping peaks into another frequency dimension (*1*). The increase in experiment time is a fair price to pay for the ability to tease out overlapping multiplets, determine connectivity, and make the necessary assignments. However, resolution in the interferometric (or indirect) dimension is limited not only by the magnet field strength, but also by the time–frequency uncertainty principle, which is part and parcel of FT signal analysis. Other limitations may include the unfavorable "phase-twist" lineshape (*2*) that arises from a purely phase-modulated set, as in homonuclear 2D *J* spectroscopy (*3*). Pressure on instrument time means that it is rarely, if ever, possible to achieve the instrumental linewidth in the interferometric dimension of a 2D experiment, especially in proton-detected heteronuclear experiments like HSQC (*4*). For example, a 1-Hz carbon-13 linewidth, typical of a natural product, would require an approximate 1-s acquisition time which, at 500 MHz, might translate into 20,000 increments! Higher magnetic field strengths exacerbate the problem by increasing the spectral width linearly, so that a 2-h 2D experiment at 400 MHz can become a 4-h 2D experiment at 800 MHz if equal digitization in the frequency domain is desired. Even if experiment time is not a strict constraint, there is a further dark side to long acquisition times in an indirect dimension: overall sensitivity falls rapidly as the tail of the decay is sampled (*1, 5*). In 3D (*6*) and 4D (*7*) experiments these problems are compounded multiplicatively, so that linewidths in each indirect dimension are dictated nearly completely by the time–frequency uncertainty principle.

One solution is to use selective pulses to excite only a single line (*9, 10*) or a narrow band (*11–14*) of signals, reducing the required number of increments. The excitation sculpting technique (*15, 16*) is particularly advantageous for these applications (*17, 18*) because of the high out-of-band suppression ratios and well-behaved phase properties of a double pulsed field gradient spin echo. Nevertheless, selective experiments usually capture only a fraction of the available information, are typically more labor intensive to set up and run, and sometimes hinge on information that is obtained from an initial survey-mode spectrum. Finally, long acquisition times in an indirect dimension will still lead to poor absolute sensitivity, even if the relative number of increments is fewer.

In this paper we outline an alternative strategy which, in some sense, *converts sensitivity into resolution.* By using the

[1] To whom correspondence should be addressed. E-mail: ajshaka@uci.edu.

1090-7807/00 $35.00

multidimensional filter diagonalization method (FDM) to obtain a parametric nonlinear fit of the multidimensional time signal, the limitations of the time–frequency uncertainty principle can be sidestepped. The success of the method depends to some extent on the type of experiment and the intrinsic sensitivity, as noise will not fit any deterministic model. However, with adequate sensitivity the gains are very noteworthy, allowing us to contemplate high-dimensional experiments that have never held any attraction previously. With the advent of FDM, sensitivity will thus become even more important than in the past, as with adequate sensitivity on the first few time increments the entire spectrum can, in some cases, be obtained. The ability to avoid sampling the tail of the interferogram, in turn, improves the theoretical sensitivity of the experiment further, allowing some 3D and 4D spectra to be collected in a small fraction of the expected time. As sensitivity has been improving at a faster rate than resolution, the emergence of FDM seems to be a particularly well timed development.

THEORY

The filter diagonalization method was first introduced by Wall and Neuhauser (*19*). Their interest was in the context of time-dependent quantum dynamics calculations. The innovation was rapidly appreciated (*20*) and subsequently made numerically more efficient (*21*). Applications to 1D NMR experiments led to the further development (*22*) of FDM, including the idea of "averaging" several calculations. Applications of multidimensional FDM to model signals (*23*) and to 2D experiments (*24–26*) showed promise, but also revealed some hidden difficulties (*26*) in the simultaneous identification of the pairs of frequencies that specify a 2D peak, difficulties which have only recently been handled fully adequately (*27*). Projections of time signals to lower-dimensionality spectra have also been found useful (*28*). The theoretical description of multidimensional FDM is to be found in the companion paper (*29*), Paper I, allowing us to telescope the treatment here into a brief summary. The reader more interested in the theoretical underpinnings is referred to Paper I (*29*).

There are several salient points that need to be made. First, FDM is, fundamentally, an extremely efficient, numerically stable way to fit the NMR time-domain data to a sum of damped sinusoids. This fitting is accomplished locally over a small region in frequency; the entire spectral range is treated by using small, overlapping frequency domains. Second, in FDM the different spectral dimensions are not independent, allowing information along one direction to improve the quality of the overall fit, and hence improve the situation in some other dimension. That is, in FDM it is integral D-dimensional features that are identified using all the available information. The approach is thus rather different than, e.g., piecemeal analysis of each dimension separately. Third, FDM is a linear algebraic technique, so that the existence and uniqueness of the results are usually guaranteed and problems with nonconvergence of the algorithm are obviated. Fourth, FDM operates on purely phase-modulated data. It is not necessary to acquire the usual pairs of sin- and cos- or N- and P-type signals. Fifth, it is unnecessary to know (or attempt to guess) the "true" number of peaks that are present. Finally, FDM is numerically efficient in the sense that, with correct numerical implementation, the algorithm shows quasi-linear scaling with respect to the total number of data points.

The fact that resolution can apparently improve by sampling along a completely different and unrelated dimension is one of the most counterintuitive features of FDM, and also one of its most desirable. This advantage compared to conventional FT analysis can depend on how well the signal is modeled as a sum of damped sinusoids. Roughly speaking, in order to achieve a good fit it is important to have an overdetermined system, in which the true number of peaks, including noise, is dominated by the total measured signal. Thus, spectra in which the final number of displayed peaks is small and the noise is low can be processed with great advantage. Spectra with nonstationary frequencies, high noise levels, or severe departure from Lorentzian lineshape are more problematical.

The general D-dimensional case is rather involved (*29*), so we will focus immediately on the interesting case $D = 2$, which shows some of the difficulties not present in the 1D case (*22*). The central quantum mechanical ansatz of FDM is to associate the measured signal $C(n_1, n_2)$ with a two-dimensional time autocorrelation function of two commuting complex symmetric Hamiltonians

$$C(n_1, n_2) = (\Phi_0 | e^{-in_1\tau_1\hat{\Omega}_1} e^{-in_2\tau_2\hat{\Omega}_2} \Phi_0) \qquad [1]$$

with the result that the task of fitting the signal to two-dimensional (phase-twist) lines is replaced with that of diagonalizing the evolution operators, $\exp(-i\tau_l\hat{\Omega}_l)$ of Eq. [1]. The corresponding matrix representations of these operators for signals of interest can be as large as $10^6 \times 10^6$, necessitating a clever strategy to diagonalize them. In the most straightforward formulation of FDM, the diagonalization is achieved by (i) setting up a localized Fourier basis to calculate the matrix elements of the evolution operators over a small 2D region in frequency space $[f_{1\min}, f_{1\max}] \times [f_{2\min}, f_{2\max}]$, producing a *small* matrix problem, and (ii) using standard library routines to solve this generalized eigenvalue problem (*29*). The result is a list of eigenvalues and eigenvectors, of $\hat{\Omega}_1$ and $\hat{\Omega}_2$, for features within the chosen region. Accuracy at the edges of the region is imperfect, necessitating overlapping windows to process the full spectral width. The total number of basis functions in the window is the product of the number allowed along the corresponding region in each frequency dimension. This number, in turn, is dictated by the length of the measured signal in this dimension, and is around half of the total number of points that would appear in the FT spectrum of the same signal, without zero-filling. While this localized Fourier basis is the simplest to

understand, we note that more subtle basis sets can be chosen if very wide lines and/or large background signals are present (*30*).

For a simulated signal exactly matching the model of discrete, purely Lorentzian features, FDM can extract, exactly, the correct spectral representation of a *D*-dimensional time signal provided that the total number of time points is sufficient. An exact "line list" (*22, 29*) can be extracted as well provided that a couple of usually weak conditions are met. When there is nonnegligible noise, the problem of identifying, or assigning, pairs of frequencies is nontrivial. This makes a correct line list more difficult to obtain directly. The source of the problem is that the eigenvectors for $\hat{\Omega}_1$ and $\hat{\Omega}_2$ become inequivalent. The noise present in the signal destroys the commutativity of the matrix representations, of these operators, that can be computed from the FID. However, a decent spectral representation of the data can still be obtained, by a direct formula in terms of Green's functions (*27, 29*) as shown in Paper I. It is also possible to compute what we term *direct projections* that correspond to linear combinations of $\hat{\Omega}_1$ and $\hat{\Omega}_2$. In particular, for 2D *J* spectroscopy the 45° projection along $\hat{\Omega}_1 - \hat{\Omega}_2$ is useful (*28*) for producing a proton-decoupled proton spectrum (*3*) without the usual lineshape problems. The beauty of this formulation is that a direct variational calculation is performed for the frequencies of interest, rather than constructing an entire 2D spectrum first, and *then* making a projection of the frequency data. The numerical aspects of direct projections are complicated, and are treated in detail in Paper I.

One of the distinct strengths of FDM is that a number of different calculations can be carried out using slightly different subsets of the data, different window sizes, etc., followed by either comparing or coadding the results. This kind of averaging tends to reinforce features that fit the model well and deemphasize noise or unwanted artifacts that are sensitive to any change in the parameters of the calculation. It is best illustrated by example spectra. The spectra shown here are, except where noted, all the result of several coadded FDM calculations, using different numbers of points along the running time, and are all what we have previously termed "ersatz" spectra. That is, they are purely synthetic spectra calculated in a deterministic way from the lists of eigenvalues and eigenvectors. Any feature not picked up by FDM would thus "disappear" from the computed spectrum. Likewise, any feature that can only be imperfectly fit as a linear combination of Lorentzian peaks would appear distorted. It is possible to ameliorate these potential problems by computing a "hybrid" spectrum (*19, 23, 25*) in which the FT of any residual difference between the calculated fit and the experimental data is added to the ersatz spectrum. However, in most cases the hybrid spectrum is superfluous, as the ersatz spectrum itself contains all the relevant information. Also, when truncation is severe, the residual difference needs to be apodized quite strongly, which in turn can limit the utility of the "correction."

EXPERIMENTAL

Spectra were obtained on a Varian UnityPlus 500-MHz spectrometer using a Varian triple-resonance probe with a shielded PFG coil to supply gradients of up to 30 G/cm along the *z* axis. The field was manually shimmed, with no special precautions taken to obtain exceptional lineshape, although receiver gain was optimized to fill the 16-bit ADC registers completely. No oversampling or digital filtering was used. The typical sensitivity obtained on this 6-year-old probe is 440:1 on a standard ethylbenzene sample, almost a factor of 2 worse than current probes can deliver. As FDM performs best when the noise level is not too high, the success of the experiments under these conditions is encouraging.

Heteronuclear Chemical Shift Correlation Spectra

It is particularly illustrative to examine the performance of 2D FDM on heteronuclear 2D spectra in which the number of increments will almost always result in significant truncation. Figure 1 shows a comparison of some ^{15}N HMQC spectra of the metalloprotein rubredoxin (*31, 32*) obtained with a modified pulse sequence (*33*) that suppresses the (poorly resolved) H_α–NH splitting. The FT spectrum was obtained in "overkill mode" using 512 increments to digitize the ^{15}N spectral width very finely. The averaged FDM spectra are obtained with 4, 8, or 16 increments. The convergence of the features in the FDM spectrum is completely different than that obtained by FT analysis of such truncated signals. Features that are relatively sharp and isolated, like the high-field resonance, are obtained essentially immediately. This fast convergence occurs because the local density of basis functions, in a window around the peak in question, is high enough to result in a very good fit of the data, with smaller components to fit the noise. On the other hand, peaks that are crowded, such as the four crowded features near 114 ppm in the ^{15}N dimension, cannot be resolved with such a short acquisition. The number of allowed basis functions, according to the criteria discussed above, may literally be less than the number of peaks to be fit, so that the result is the best fit obtained using, say, only three peaks. This observation, namely that it is more difficult to resolve closely spaced peaks than to obtain a narrower linewidth for an isolated peak, is a good check on claims of improved resolution by any algorithm. There are ways to check the convergence of FDM, one of the most straightforward being to compute spectra from signals of different lengths in the indirect dimension and visually inspect the results. Once a feature has stabilized, it acquires an added measure of reliability. Of course it is always possible that an apparent singlet consists of two closely spaced peaks, with a splitting much smaller than can be resolved.

The important role of averaging is illustrated by the spectra in Fig. 2. The first two panels are FDM ersatz HMQC spectra of rubredoxin using 32×60 and 32×100 points for the

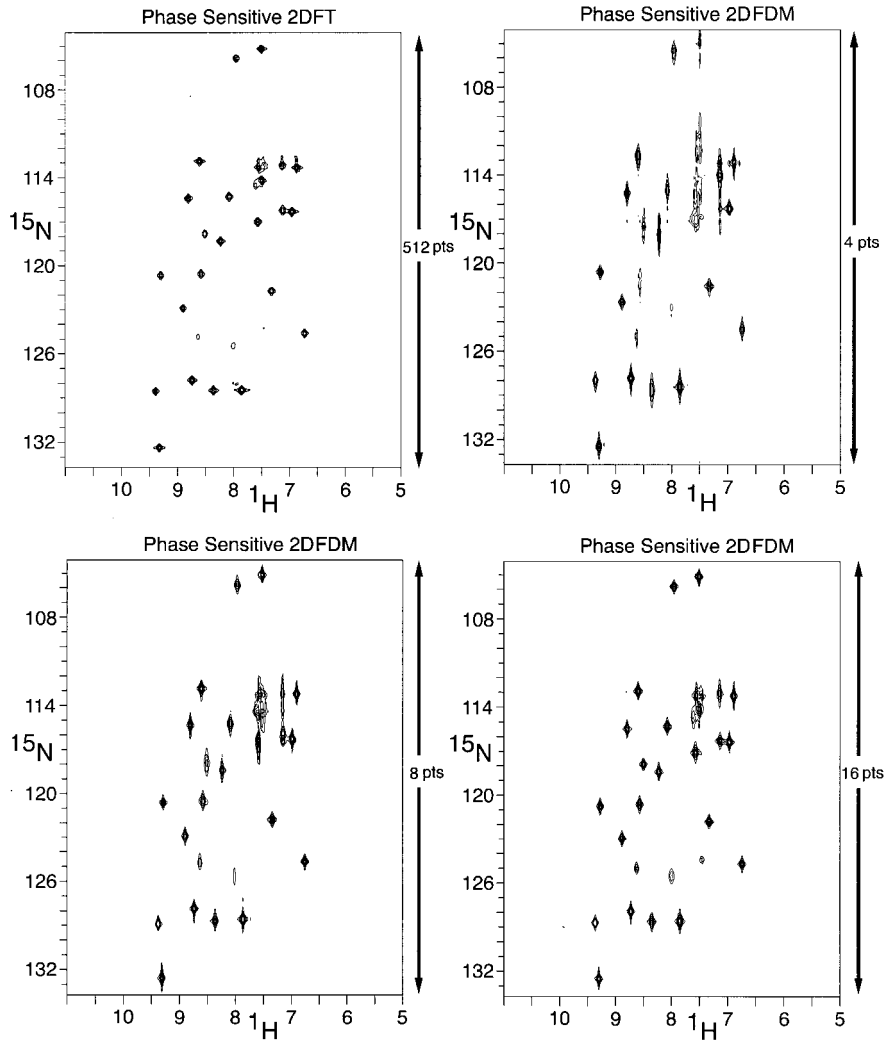

FIG. 1. ^{15}N–^{1}H HMQC spectra of nitrogen-15-labeled (100%) rubredoxin, a 4.5-kDa metalloprotein, obtained in 90% H_2O/10%D_2O at 25°C. The top left panel shows the FT spectrum obtained with 512 increments and minimal apodization in the ^{15}N dimension. A 10-Hz line broadening in the proton dimension was employed. The other three panels show the (averaged) FDM ersatz spectra obtained with only 4, 8, or 16 points. Most of the resonances are immediately resolved, with a denser cluster near (7.4,114) ppm. These features start to emerge more clearly in the 16-point spectrum.

calculation, respectively. In addition to the expected peaks, there is a host of smaller artifacts that appear (*29*) and are a natural outcome of the Green's function formula used to compute the spectrum from the two distinct lists of eigenvalues for $\hat{\Omega}_1$ and $\hat{\Omega}_2$, respectively. These small peaks can be viewed as the result of a combination of any departure from a purely Lorentzian noise-free signal, and the use of a formally incomplete basis. If the operators $\hat{\Omega}_1$ and $\hat{\Omega}_2$ could be simultaneously diagonalized, the artifacts would vanish. However, when the matrix representations of the operators in the window basis do not commute, such simultaneous diagonalization is not possible. Fortunately, in the two calculations the artifacts show a random appearance in both position and phase: They may thus be reduced by simply coadding the ersatz spectra from different calculations. The third spectrum shows the FDM ersatz spectrum obtained by coaddition of 26 calculations, $32 \times 60 \ldots 32 \times 100$, in which the stable, true peaks have survived and the direct product peaks have been attenuated. Compared to an FT spectrum, which requires a minimum of 128 points, a factor of at least 4, and possibly 6, in time for data acquisition is obtained. This factor could be radically improved by "zooming in" on the crowded region in the nitrogen-15 using excitation sculpting to discard all peaks outside. Two spectra, with only four increments each, could then suffice to characterize all the information.

Averaging, as described above, is a numerically expensive option that may not always be applicable, and we would prefer to avoid it altogether. However, attempting to discard the artifacts according to some prespecified criterion has not been particularly promising. For one thing, the genuine features may also be slightly distorted in any single realization of the ersatz spectrum, and so one would also need to correct *them* after

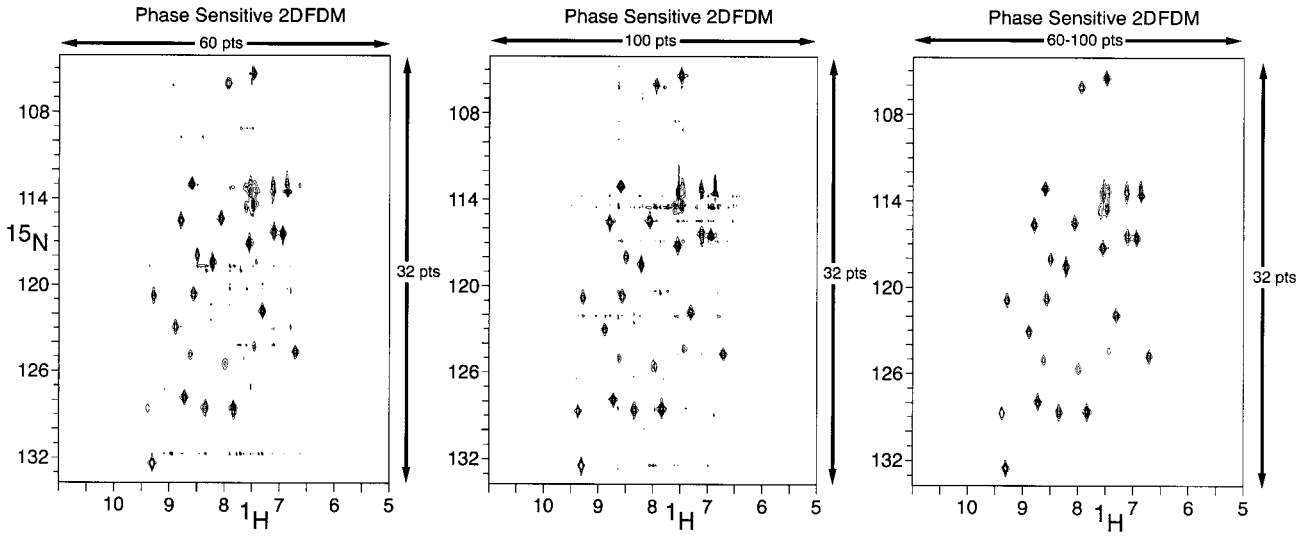

FIG. 2. The importance of averaging. The same data as Fig. 1 is shown, now with 32 increments. The two left-hand plots show the FDM ersatz spectrum from a single calculation using either 60 points or 100 points along the proton direction. Small artifacts, many of which are out of phase, appear as streaks. These small peaks arise from the formula used to compute the 2D ersatz spectrum. The third spectrum results from the addition of 21 ersatz spectra spanning this interval. It compares favorably with the fully converged FT spectrum.

purging the unwanted peaks. Attempting to identify *pairs* of eigenvalues, and so eliminate the artifacts up front, is a laudatory goal (*24*, *26*) that unfortunately is still slightly out of reach for all except the most ideal signals. In addition, such a scheme would become ever more tedious to implement in higher-dimensional spectra. Other methods to regularize the spectrum will be discussed in future publications.

HSQC and Singlet-HSQC Spectra

The potential of multidimensional FDM can be brought into stark relief by calculating a phase-sensitive absorption-mode ersatz spectrum that would be exceedingly difficult to obtain otherwise, and that will prove to be useful for the analysis of medium-sized organic molecules. The spectrum incorporates all the features discussed previously: absorption-mode spectra from purely phase-modulated signals, resolution that far exceeds that expected according to the time–frequency uncertainty principle, and direct projection along a nontrivial time direction to achieve radical simplification of the spectrum. We call the resulting 2D spectrum a *singlet*-HSQC spectrum, as each C–H correlation appears as a single resonance at the coordinates of their respective chemical shifts.

The pulse sequence timing diagram is shown in Fig. 3. It is a slightly modified HSQC sequence (*4*) using gradient selection (*34*) of the desired coherence transfer pathway (*35*). All phase shifts in the carbon-13 dimension are removed by using a CLUB sandwich (*36*) for phase encoding rather than a conventional PFG. The open icons are 180° pulses. The scored icons signify high-power constant-amplitude frequency-modulated inversion pulses of duration 60 μs on ^{1}H and 112 μs on ^{13}C, and have been described previously (*24*, *36*). Following the reverse polarization transfer step, an additional (double) spin echo adds a homonuclear J dimension (here t_3 and F_3), after which the decoding PFG and rephasing of the direct CH coupling are included as usual. Potential diffusion losses could accrue if the total time between the PFG encode/decode steps is too long. However, only a short J evolution time of maximum 20 ms is required, corresponding to a single nonzero time delay for the 50-Hz spectral width in the J dimension, so the diffusion losses are negligible with the gradient strengths em-

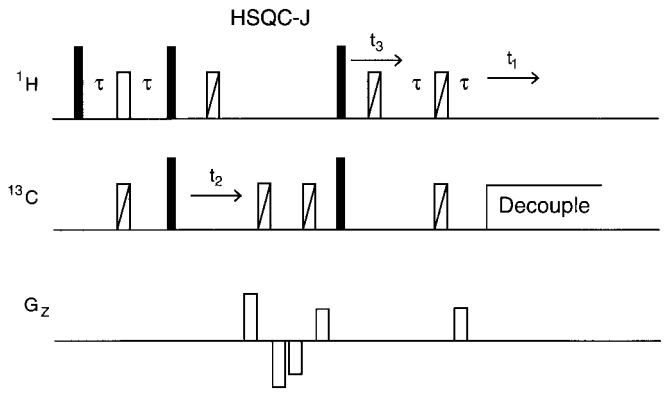

FIG. 3. Pulse sequence timing diagram for the HSQC-J experiment that yields a *singlet*-HSQC spectrum. Solid and open icons are conventional 90° and 180° pulses. The 90° pulse width was 10 μs on protons and 14 μs on carbon-13. The scored icons are full-power constant-amplitude FM pulses. The delay $\tau = 1/4^{1}J_{CH}$ was set to 1.8 ms. The CLUB sandwich uses two pairs of antiphase gradients to encode the carbon-13 magnetization. These four PFGs have, in absolute value, four times the area of the single decode PFG applied after the final FM 180° pulses.

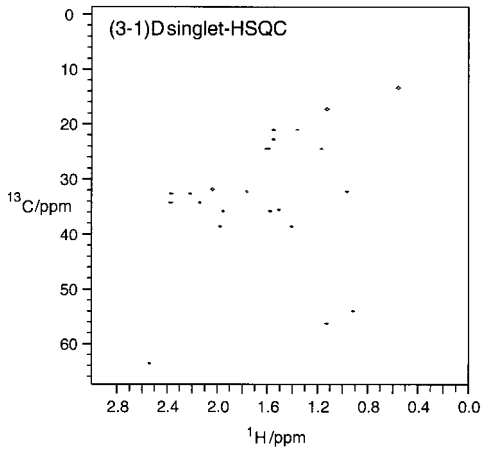

FIG. 4. The *singlet*-HSQC spectrum of progesterone, obtained using the pulse sequence of Fig. 3. The 3D data set consisted of 1024 × 64 × 2 in the proton, carbon-13, and proton *J* dimensions, respectively. The spectrum is purely phase modulated in each of the indirect dimensions. The broad proton multiplets characteristic of the extended network of spin–spin coupling in this steroid have been condensed to nearly structureless singlets at the appropriate chemical shifts.

ployed. Carbon-13 decoupling is only initiated at the beginning of acquisition, as it can interfere with proper echo formation.

Figure 4 shows a natural abundance (3-1)-dimensional *singlet*-HSQC spectrum of progesterone, in which the notation $(n - m)$ denotes the dimensionality of the time-domain data (n) and frequency-domain data $(n - m)$. Two purely phase-modulated HSQC spectra ($t_3 = 0$ and $t_3 = 20$ ms) each with $N_2 = 64$ increments over a spectral width of 8625 Hz in the carbon-13 dimension were obtained and the Green's function spectral representation was calculated using 50 FDM computations with proton points $N_1 = 502, 504, \ldots, 600$ (averaged together) to obtain the displayed result. All proton–proton couplings have been removed, leading to a radical improvement in resolution. Strong coupling effects are noticeably absent in the spectrum, even though progesterone has many protons within a narrow chemical shift range. The lack of strong coupling effects arises from several factors. First, magnetization transfer from a directly attached proton to a neighbor by the mixing effect of a 180° pulse to a strongly coupled spin system may not result in a detectable signal in the natural ^{13}C abundance case because the signal may remain antiphase with respect to the carbon-13 coupling. Second, in FDM a phase-sensitive projection is obtained: the strong coupling artifacts have both algebraic signs, and tend to project to zero much more readily than in absolute-value FT projections that are more familiar.

The overlay of Fig. 5 shows a zoomed spectral region around the low-field methyl-21 group. The light gray traces are contours from the absolute-value FFT spectrum with 64 increments in the carbon-13 dimension, using only the first point in the *J* dimension. The resolution is poor on account of the phase-twist lineshape and the rather scant digital resolution. The sharp black contours are from the *singlet*-HSQC spectrum, using both *J* points. Note that this spectrum can be acquired in the same time as a conventional phase-sensitive spectrum, as we do not have to obtain paired *N*- and *P*-type data sets. The absolute-value 45° FFT projection would show truly awful resolution of at least 100 Hz in the proton dimension from the projection of a 3D phase twist. Yet, using this same data, multidimensional FDM delivers a beautiful high-resolution decoupled spectrum, with very sharp lines. Note how it is information content of the time signal, in aggregate, that is important for the FDM processing. An additional dimension, even one that would be essentially worthless in an FT context, can still be very useful in multidimensional FDM. The improvement shown is not "cosmetic," as there is no easy way to divine the true number of signals present, even in a phase-sensitive FT spectrum, using only 64 increments. In the absolute-value FT spectrum, there is only the roughest indication of the underlying structure in the crowded regions, and no way to conclusively identify the peaks.

Figure 6 shows a comparison of one vertical trace and one horizontal trace from the data in Fig. 5, except that both *N*- and *P*-type data sets were combined in the usual way to obtain an absorption-mode FT spectrum. The vertical trace shows the improvement in resolution along the carbon-13 dimension, while the horizontal trace illustrates the collapse of the proton multiplets for a pair of inequivalent methylene protons. The resolution is markedly improved, as expected from the contour plot. The resonances have different widths but similar 2D volume integrals. Using only a single *J* increment, the projection produces a close cluster of nearly degenerate poles for each peak, with each pole having slightly different linewidth. It appears that wider and more complex proton multiplets are harder to "decouple" although no spurious splittings appear. Given results like these on an organic molecule of modest

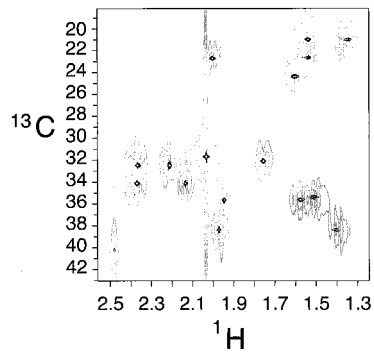

FIG. 5. A comparison of the absolute-value 1024 x 64 conventional HSQC spectrum (light gray contours) with the *singlet*-HSQC spectrum was obtained as described in the text using 50 FDM calculations 502 × 64 × 2, . . . , 600 × 64 × 2 on a subset of the data (narrow black contours). There is nothing special about this choice of parameters for averaging, with no attempt being made to optimize them. Similar results are obtained using, e.g., 20 coadded ersatz spectra. Every peak is correctly identified, and the improvement in resolution is remarkable.

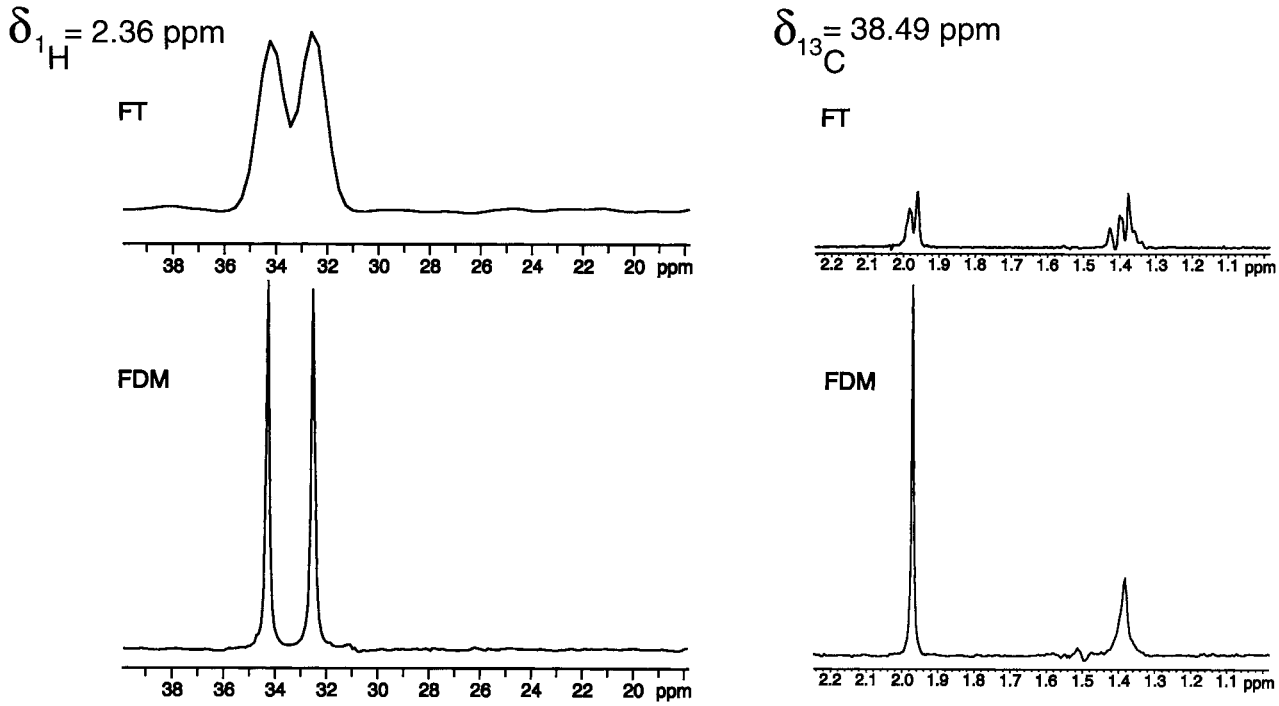

FIG. 6. Traces extracted from the 2D spectrum shown in Fig. 5. The left-hand pair shows the conventional FFT (top) and FDM (bottom) vertical traces at the proton shift of 2.36 ppm, where there are two rather closely spaced carbon-13 resonances. The right-hand pair shows the improved resolution along the proton dimension, at the carbon-13 shift of 38.49 ppm, where a pair of inequivalent methylene protons are seen. The collapse of the multiplet structure in the *singlet*-HSQC makes assignment and measurement of the chemical shifts a fairly easy job. The two protons have somewhat different linewidths, even after 1 Hz smoothing, although there is no evidence for any residual multiplet structure on either line.

complexity, we foresee the *singlet*-HSQC spectrum as perhaps one of the most attractive new experiments to employ for routine characterization whenever enough material is available to achieve decent signal-to-noise ratio.

Homonuclear Correlation Spectra: Singlet-TOCSY

In 2D correlation spectra like TOCSY, the telltale cross peaks invariably consist of a cluster of closely spaced multiplet components. If the mixing sequence produces a nearly pure isotropic average Hamiltonian $\bar{\mathcal{H}} = \mathcal{H}_J$ as, for example, the DIPSI-2 sequence (*37*, *38*) does, then not all the transitions within the 2D multiplets of simple spin systems are of equal intensity (*39*). However, pulse imperfections, and spin-locking segments used to purge out-of-phase magnetization, can lead to almost all the possible lines appearing, giving wide rectangular multiplet patterns in practice. We show here how these 2D multiplets can be condensed to singlets using multidimensional FDM.

A substantial improvement in resolution would result if the multiplets could be "decoupled" in both dimensions, leading to sharp singlets at the intersection of the corresponding chemical shifts of the two spins involved, and with intensity that is the integral of the entire multiplet. Decoupling the diagonal peaks would help to improve the resolution near the diagonal, as well. This decoupling in both dimensions can be achieved by conducting a 4D time-domain experiment we call *J*-TOCSY-*J*, in which there is a homonuclear *J* dimension prior to each of the normal time dimensions in a conventional TOCSY experiment. A double 45° projection of the 4D time signal then leads to a (4-2)D result we call *singlet*-TOCSY.

Figure 7 shows the pulse sequence timing diagram for the *J*-TOCSY-*J* experiment, with Fig. 8 displaying a preliminary application of the experiment to a trivial case of three weakly coupled protons. It is possible to decouple each dimension separately, or both together, from one 4D time signal. Note that the TOCSY spectrum has many exactly degenerate peaks, so

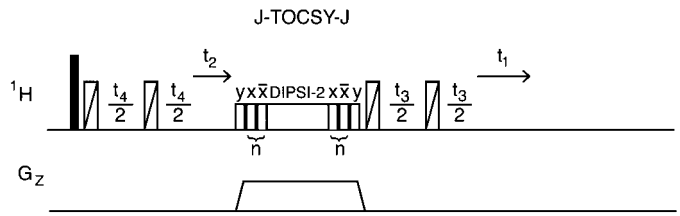

FIG. 7. Pulse sequence timing diagram for the *J*-TOCSY-*J* experiment, capable of producing a *singlet*-TOCSY spectrum. The sequence is a conventional TOCSY sequence with short purging sections that consist of a *y*-phase spin lock and a short Tr-ROESY sequence. The purging makes the conventional TOCSY spectrum more appealing cosmetically, as most dispersive contributions are removed. The PFG is about 0.5 G/cm, ramped up during the purging and maintained during the DIPSI-2 sequence.

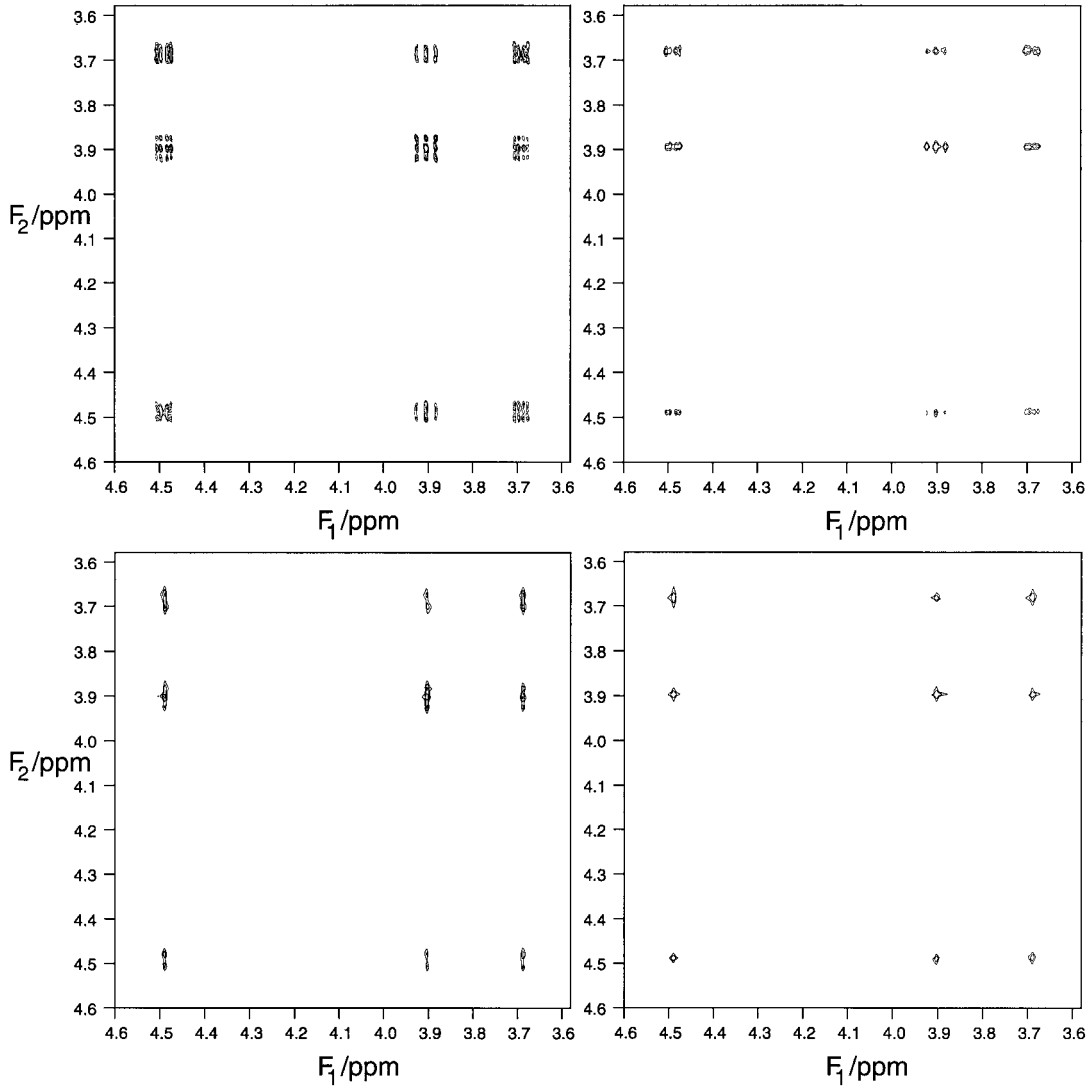

FIG. 8. Successive simplification of 2D TOCSY spectra. All the spectra have been obtained with the pulse sequence of Fig. 7 using a 5-kHz RF field during the mixing time. The spin lock is 40 ms, the Tr-ROESY purging sequence is 35 ms, and mixing time for DIPSI-2 is 53 ms. The upper left panel is the conventional phase-sensitive 2D TOCSY spectrum obtained with a data matrix of 80 FIDs, each 200 complex points in length, zero-filled to 256 × 1024 prior to Fourier transformation. Gaussian apodization has been employed to attenuate any truncation artifacts. The other three panels show the effect of decoupling along F_1, F_2, and, finally, both F_1 and F_2. (Here F_1 is the running time.) As described in the text, enough smoothing has been applied to generate decent contours without using prohibitively high digital resolution. The unsmoothed ersatz spectra can have linewidths that approach zero, as the phase-sensitive FDM projection along each *J* dimension subtracts both frequencies *and* widths (the frequencies in FDM are always complex). Only a single increment along t_3 and t_4 was needed. These phase-sensitive spectra are, of course, impossible to obtain with FT processing—or any other method we are aware of.

that it is impossible to use a very small number of increments in the usual indirect chemical shift dimension, as is sometimes possible in the HSQC case, because we are attempting to quantify several degenerate peaks. Nevertheless, it is neither necessary to fully resolve the 2D multiplet structure, nor to have purged spectra without any dispersive components, for the experiment to succeed. We obtained similar results with a conventional *z*-TOCSY (*40*) experiment without any attempt to remove zero-quantum coherence. Any antiphase dispersive components tend to project to a null signal when the multiplet collapses. The *J* dimensions can, in principle, be obtained with only a single nonzero increment, so that only *three* 2D TOCSY spectra are required to obtain the singlet spectrum, the method actually used in Fig. 8.

In Fig. 9 corresponding vertical cross sections through the central part of the central triplet, in the TOCSY and *singlet*-TOCSY spectra, are compared. Along the indirect dimension the multiplet components are not resolved. In the decoupled spectra enough smoothing is applied to get a decent appearance. This is necessary because the subtraction of complex frequencies leads to a subtraction of the corresponding widths, i.e., the difference between the linewidth in the *J* dimension

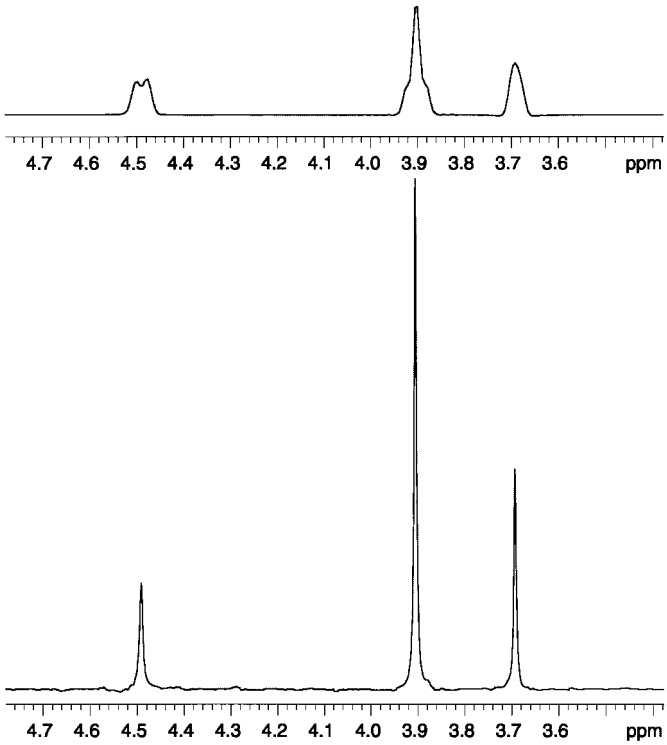

FIG. 9. Traces along the interferometric dimension, at the position of the central peak of the triplet, the center multiplet. The top trace shows the (poorly resolved) multiplet structure that is characteristic of typical TOCSY spectra. The bottom trace shows the corresponding *singlet*-TOCSY spectrum, in which sharp resonances are observed. The intensities are, of course, somewhat arbitrary, as they depend on the mixing time employed in the experiment, and the values of all the couplings.

and the associated chemical shift dimension. We used a Lorentzian smoothing, although it is equally possible to employ convolution with a Gaussian function to obtain elliptical contours. As there are many other issues that need to be addressed with respect to the optimum way to conduct the experiment for more realistic and crowded spectra, a more complete description of the experiment, highlighting these issues, will be forthcoming.

SUMMARY

Multidimensional FDM is a timely development, with a huge number of potential applications. It can be used to minimize spectrometer time whenever digitization, as opposed to true sensitivity, is the primary limitation. It can also be used to produce exciting new spectra that are particularly clear and straightforward to interpret. The results shown here are still only preliminary, and there are many further improvements that can be envisioned, both theoretically and experimentally. These augmentations will follow in further work, now underway, on the application of FDM to multidimensional NMR experiments.

ACKNOWLEDGMENTS

This work was supported by the National Science Foundation, CHE-9900422, and by a UC BioSTAR grant, S97-18.

REFERENCES

1. R. R. Ernst, G. Bodenhausen, and A. Wokaun, "Principles of Nuclear Magnetic Resonance in One and Two Dimensions," Clarendon Press, Oxford (1987).
2. G. Bodenhausen, R. Freeman, R. Niedermeyer, and D. L. Turner, Double Fourier transformation in high-resolution NMR, *J. Magn. Reson.* **26,** 133–164 (1977).
3. W. P. Aue, J. Karhan, and R. R. Ernst, Homonuclear broad band decoupling and two-dimensional *J*-resolved NMR spectroscopy, *J. Chem. Phys.* **64,** 4226–4227 (1976).
4. G. Bodenhausen and D. J. Ruben, Natural abundance nitrogen-15 NMR by enhanced heteronuclear spectroscopy, *Chem. Phys. Lett.* **69,** 185–189 (1980).
5. M. H. Levitt, G. Bodenhausen, and R. R. Ernst, Sensitivity of two-dimensional spectra, *J. Magn. Reson.* **58,** 462–472 (1984).
6. C. Griesinger, O. W. Sørensen, and R. R. Ernst, Three-dimensional Fourier spectroscopy. Application to high-resolution NMR, *J. Magn. Reson.* **84,** 14–63 (1989).
7. L. E. Kay, G. M. Clore, A. Bax, and A. M. Gronenborn, Four-dimensional heteronuclear triple-resonance NMR spectroscopy of Interleukin-1β in solution, *Science* **249,** 411–414 (1990).
8. Deleted in proof.
9. A. J. Shaka and R. Freeman, Selective excitation of proton spectra by polarization transfer from an adjacent carbon site, *J. Magn. Reson.* **50,** 502–507 (1982).
10. C. Bauer and R. Freeman, Decomposition of proton NMR spectra into individual spin multiplets, *J. Magn. Reson.* **61,** 376–381 (1985).
11. H. Geen and R. Freeman, Band-selective radiofrequency pulses, *J. Magn. Reson.* **93,** 93–141 (1991).
12. H. Geen and R. Freeman, Band-selective excitation for multidimensional NMR spectroscopy, *J. Magn. Reson.* **87,** 415–421 (1990).
13. C. Roumestand, D. Canet, N. Mahieu, and F. Toma, DANTE-Z, an alternative to low-power soft pulses. Improvement of the selection scheme and applications to multidimensional NMR studies of proteins, *J. Magn. Reson. A* **106,** 168–181 (1994).
14. B. Brutscher, J. P. Simorre, and D. Marion, Optimization of multidimensional NMR using band-selective pulses, *J. Magn. Reson.* **100,** 416–424 (1992).
15. T. L. Hwang and A. J. Shaka, Water suppression that works. Excitation sculpting using arbitrary waveforms and pulsed field gradients, *J. Magn. Reson. A* **112,** 275–279 (1995).
16. K. Stott, J. Keeler, T. L. Hwang, and A. J. Shaka, Excitation sculpting in high-resolution nuclear magnetic resonance spectroscopy—Application to selective NOE experiments, *J. Am. Chem. Soc.* **117,** 4199–4200 (1995).
17. V. V. Krishnamurthy, Application of semi-selective excitation sculpting for homonuclear decoupling during evolution in multidimensional NMR, *Magn. Reson. Chem.* **35,** 9–12 (1997).
18. Q. N. Van and A. J. Shaka, Improved cross peak detection in two-dimensional proton NMR spectra using excitation sculpting, *J. Magn. Reson.* **132,** 154–158 (1998).
19. M. R. Wall and D. Neuhauser, Extraction, through filter-diagonalization, of general quantum eigenvalues or classical normal mode frequencies from a small number of residues or a short-time seg-

ment of a signal. I. Theory and application to a quantum-dynamics model, *J. Chem. Phys.* **102,** 8011–8022 (1995).

20. V. A. Mandelshtam and H. S. Taylor, Spectral analysis of time correlation function for a dissipative dynamical system using filter diagonalization: Application to calculation of unimolecular decay rates, *Phys. Rev. Lett.* **78,** 3274–3277 (1997).
21. V. A. Mandelshtam and H. S. Taylor, Harmonic inversion of time signals and its applications, *J. Chem. Phys.* **107,** 6756–6769 (1997).
22. H. Hu, Q. N. Van, V. A. Mandelshtam, and A. J. Shaka, Reference deconvolution, phase correction and line listing of NMR spectra by the 1D filter diagonalization method, *J. Magn. Reson.* **134,** 76–87 (1998).
23. V. A. Mandelshtam and H. S. Taylor, Multidimensional harmonic inversion by filter-diagonalization, *J. Chem. Phys.* **108,** 9970–9977 (1998).
24. V. A. Mandelshtam, H. Hu, and A. J. Shaka, Two-dimensional HSQC NMR spectra obtained using a self-compensating double pulsed field gradient and processed using the filter diagonalization method, *Magn. Reson. Chem.* **36,** S17–S28 (1998).
25. V. A. Mandelshtam, H. S. Taylor, and A. J. Shaka, Application of the filter diagonalization method to one- and two-dimensional NMR spectra, *J. Magn. Reson.* **133,** 304–312 (1998).
26. M. R. Wall, T. Dieckmann, J. Feigon, and D. Neuhauser, Two-dimensional filter-diagonalization: Spectral inversion of 2D NMR time-correlation signals including degeneracies, *Chem. Phys. Lett.* **291,** 465–470 (1998).
27. V. A. Mandelshtam, H. Hu, N. D. Taylor, M. Smith, and A. J. Shaka, Highly resolved double absorption 2D NMR spectra from complex severely truncated 2D phase-modulated signals by filter-diagonalization-averaging method, *Chem. Phys. Lett.* **305,** 209–216 (1999).
28. V. A. Mandelshtam, Q. N. Van, and A. J. Shaka, Obtaining proton chemical shifts and multiplets from several 1D NMR signals, *J. Am. Chem. Soc.* **120,** 12161–12162 (1998).
29. V. A. Mandelshtam, The multidimensional filter diagonalization method. I. Theory and numerical implementation, *J. Magn. Reson.* **144,** 343–356 (2000).
30. J. Chen and V. A. Mandelshtam, Multi-scale filter diagonalization method for spectral analysis of noisy data with non-localized features, *J. Chem. Phys.* **112,** 4429–4437 (2000).
31. B. F. Volkman, A. M. Prantner, S. J. Wilkens, B. Xia, and J. L. Markley, Assignment of H-1, C-13, N-15 signals of oxidized *Clostridium pasteurianum* rubredoxin, *J. Biomol. NMR* **10,** 409–410 (1997).
32. A. M. Prantner, B. F. Volkman, S. J. Wilkens, B. Xia, and J. L. Markley, Assignment of H-1, C-13, and N-15 signals of reduced *Clostridium pasteurianum* rubredoxin: Oxidation state-dependent changes in chemical shifts and relaxation rates, *J. Biomol. NMR* **10,** 411–412 (1997).
33. H. Hu, M. Smith, and A. J. Shaka, The HMQC experiment revisited. Semiselective pulses and double resonance modifications, to be submitted.
34. R. E. Hurd and B. K. John, Gradient-enhanced proton-detected heteronuclear multiple-quantum coherence spectroscopy, *J. Magn. Reson.* **91,** 648–653 (1991).
35. G. Bodenhausen, H. Kogler, and R. R. Ernst, Selection of coherence-transfer pathways in NMR pulse experiments, *J. Magn. Reson.* **58,** 370–388 (1984).
36. H. Hu and A. J. Shaka, Composite pulsed field gradients with refocused chemical shifts and short recovery time *J. Magn. Reson.* **136,** 54–62 (1999).
37. A. J. Shaka, C. J. Lee, and A. Pines, Iterative schemes for bilinear operators: Application to spin decoupling, *J. Magn. Reson.* **77,** 274–293 (1988).
38. S. P. Rucker and A. J. Shaka, Broadband homonuclear cross polarization in 2D NMR using DIPSI-2, *Mol. Phys.* **68,** 509–517 (1989).
39. M. L. Remerowski, S. J. Glaser, and G. P. Drobny, A theoretical study of coherence transfer by isotropic mixing. Calculation of pulse sequence performance for systems of biological interest, *Mol. Phys.* **68,** 1191–1218 (1989).
40. M. Rance, Improved techniques for homonuclear rotating-frame and isotropic mixing experiments, *J. Magn. Reson.* **74,** 557–564 (1987).